

Integrating GPR and RIP Methods for Water Surface Detection of Geological Structures

Chieh-Hou Yang^{1,*}, Lun-Tao Tong², and Chun-Yi Yu¹

(Manuscript received 2 June 2004, in final form 26 April 2006)

ABSTRACT

Geophysical surveying in water-covered and swampy areas is particularly challenging. This paper presents a new survey strategy for such surveying that integrates ground penetrating radar (GPR) and resistivity image profiling (RIP) methods at the water surface to investigate geologic structures beneath rivers, ponds, and swamps.

Two test sites, a pond and a lake, have been selected to evaluate this new survey strategy. Experiments in both areas have been successful in delineating the structure of underlying gravel layers. The depth of water and shallow structures obtained from GPR data provided an effective constrain during processing of RIP data. Deeper structures were delineated using RIP data. The integration of GPR and RIP methods conducted at the water surface was successfully applied to map the Hsincheng fault cross-cutting the Tournayan River in Hsinchu County.

This paper shows that the use of GPR and RIP at the water surface is efficient in mapping geological structures beneath water. The proposed approach suggests the potential for conducting geophysical surveys along rivers and drainage canals in urban areas, places where roads and buildings impede other methods designed to detect active fault.

(Key words: GPR, RIP, Active fault mapping, Underwater stratigraphy)

1. INTRODUCTION

The concept of resistivity surveying is based on potential field measurement; however,

¹ Institute of Geoinformatics and Disaster Reduction Technology, Chung Yun University, Chung-Li, Taiwan, ROC

² Energy and Environment Laboratories, Industrial Technology Research Institute, Hsinchu, Taiwan, ROC

* *Corresponding author address:* Prof. Chieh-Hou Yang, Institute of Geoinformatics and Disaster Reduction Technology, Chung Yun University, Chung-Li, Taiwan, ROC; E-mail: yang@cyu.edu.tw

resistivity data from water-covered areas is influenced by the water layer (Loke 2000). For water-covered areas, electrodes can be installed at the bottom of the water to increase emitting current to the earth and sensitivity to the subsurface anomaly. However, such an approach is cumbersome and consequently expensive and time-consuming. Floating electrodes can also be utilized to increase the efficiency of field-work (Kwon et al. 2005); in which case, resistivity and the shape of the water layer must be described accurately to get a precise subsurface image. Previously, echo sounders have been used to constrain water depth when conducting continuous-resistivity profiling (CRP) at the water surface (Belaval et al. 2003).

Ground penetrating radar (GPR) has been successfully employed to map water depth and underwater stratigraphy in shallow lakes and rivers filled with fresh water (Annan and Davis 1977). Such applications challenge the myth that GPR cannot work in water. Usually, GPR provides accurate depth of water and some useful information beneath the water layer (Delaney et al. 1992).

Resistively image profiling (RIP) is a newly developed multi-electrode method that has been successfully used in land surveys. It is particularly suitable for areas where lateral variations of geological structure have rendered vertical electrical sounding (VES) unsuitable (Griffiths and Barker 1993).

RIP can provide relatively more lateral and vertical information on sub-water strata than conventional DC sounding (Loke 2000). It improves survey efficiency by performing measurements at the surface of the water; and topographic effect can be eliminated when conducting such measurements. By considering the advantages of conducting resistivity surveying at the water surface and increasing the accuracy of water thickness measurement, this study advances the use of GPR and RIP in water-covered areas. The reliability of RIP inversion is improved by incorporating water depth obtained from GPR. Taking advantage of this, a new survey strategy to improve understanding of subsurface geologic conditions in water-covered areas via GPR and RIP surveying is investigated.

Two test sites, a pond and a lake, were selected to evaluate this new survey strategy. Both of these sites are located in gravel-covered areas. The purpose of these experiments was to test the concept, develop floating electrodes, and establish a suitable flow chart for data processing. As an additional illustration, the crosscutting of the Hsincheng fault through the Tourchyan River of Hsinchu County was mapped.

2. SURVEY METHODS

2.1 Ground Penetrating Radar

GPR is widely applied in many fields. Electromagnetic (EM) energy is injected into the ground and the subsurface imaged from the returning EM signal. Due to the use of high-frequency electromagnetic waves, the resolution of GPR is very high compared with other traditional geophysical methods. However, GPR's shortcoming is that it is limited in its penetration depth; this problem relates to ground conductivity. As it is portable, efficient, and of high resolution, GPR has become a useful tool for constructing detailed images of shallow

structures (Savvaïdis et al. 1999; Lmai et al. 1987).

The pulse EKKO-100 GPR system manufactured by Sensor & Software Inc. was used in this study. A 100 MHz antenna was carried by a plastic raft floating on the water's surface, attached to a rope that constituted the desired survey line. The offset between transmitter and receiver was 1 m and the stack number of each trace was 128.

2.2 Resistivity Image Profiling

RIP method was developed to investigate complex subsurface structures, especially in areas where conventional DC sounding and other prospective methods are unsuitable (Griffiths and Barker 1993). Numerous electrodes are inserted into the soil, along the desired survey line. Two current-injected electrodes and two potential measuring electrodes are automatically selected and switched by the control unit of the resistivity meter. A rough image of a subsurface can then be created from apparent resistivity pseudosection prior to digital data processing. The resistivity depth profile can be obtained by applying 2D finite-element inversion (Loke and Barker 1996).

The McOhm-21 multi-functional resistivity meter manufactured by OYO and a pole-pole electrode configuration were used in this study. Remote current and potential electrodes were placed at a distance 10 times the expected depth of investigation, away from the survey line. An electrode cable with electrodes at 1-m intervals and PVC bottles linked to each electrode to prevent the cable from sinking were used. Electrodes were kept in good contact with the water to ensure injection of electric current into the strata through the water.

3. FIELD SURVEY STRATEGY TESTS

Two test sites were selected and both GPR and RIP were performed to evaluate the concept of measurement at water surface.

3.1 Pond Test Site

A 30 × 45 m fishing pond located 2 km away from the National Central University campus was selected as one test site. The pond had been remodeled just prior to this test. The bottom of the pond is covered with pebbles, while the upper layer of ground is of Quaternary laterite deposit of approximately 3- to 4-m thickness. Beneath the laterite layer is a gravel layer with a thickness from 10 to 20 m. Underlying the gravel layer are alternating sand and clay layers. The depth of the groundwater table is greater than 10 m.

A 39-m survey line was set on the water's surface in a N-S direction and two Schlumberger VES were performed at the north and south end of the pool to verify stratigraphic conditions. As shown in Fig. 1, the maximum half spacing of these two VES was 30 m. A 1-D inversion was applied to these two soundings. The top soil/laterite had a thickness of less than 1 m, with a resistivity ranging from 39.4 to 146 ohm-m. The stratum underlying the laterite is a gravel layer with a thickness of 8.8 to 13.5 m and a resistivity of 283 to 366 ohm-m. The layer

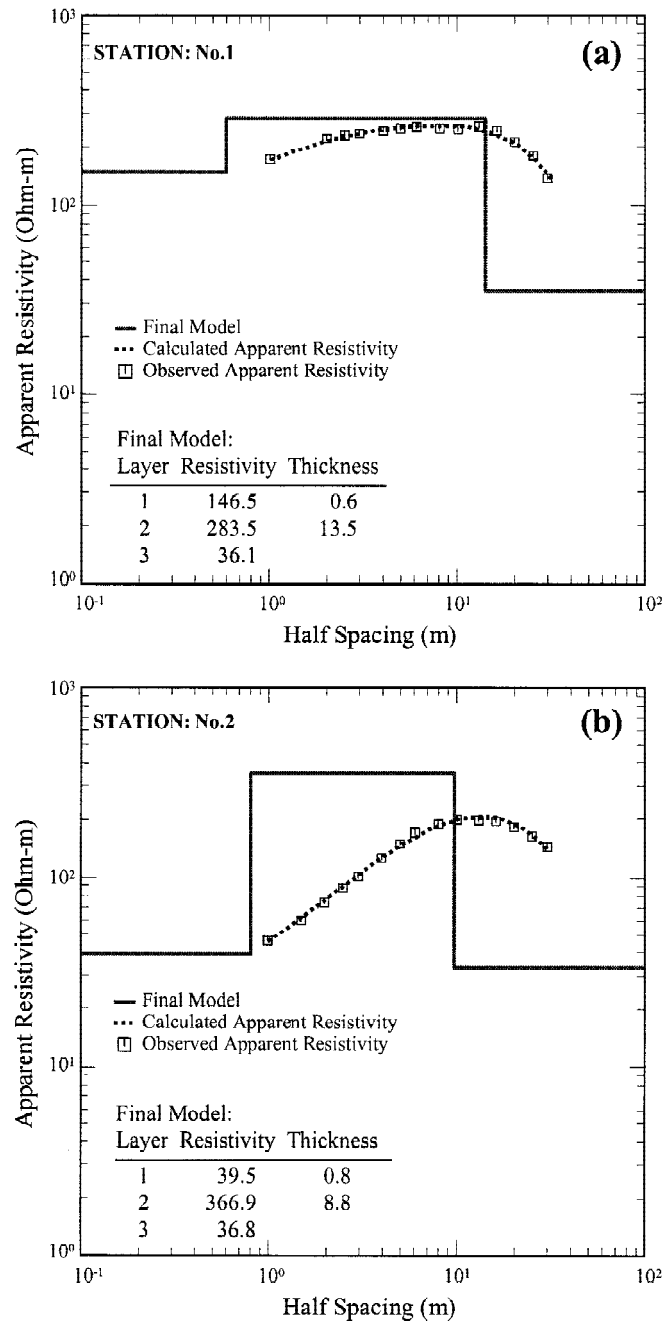


Fig. 1. Schlumberger vertical electrical sounding (VES) curves collected at the (a) northern (b) southern sides of the fishpond.

beneath the gravel layer has a resistivity of 36.1 to 36.8 ohm-m and serves as a potential aquifer for this area.

Figure 2a shows the GPR image of the survey line on the water's surface. The depth of the pond's bottom ranges from 2.5 to 2.7 m, gently deepening from north to south. Obvious diffraction along the bottom was caused by pebbles. Because radar waves cannot penetrate far beyond the water's bottom, only limited information beneath the pebble bottom can be obtained. Figure 2b shows an apparent resistivity pseudosection with the same profile as GPR. The pseudosection shows a fairly uniform gradation of apparent resistivity across the section with some expected distortion at the edges.

Figure 2c shows the inverted resistivity depth section from 2D finite-element inversion. The root-mean-square error is 2.1% after 5 iterations. Resistivity increased as the water deepened. As shown in Fig. 2c, the thickness of mud/wet laterite underneath the pebble bottom is less than 2 m with a resistivity ranging from 80 to 200 ohm-m. The stratum underneath the laterite is a gravel layer with a resistivity greater than 200 ohm-m and a thickness greater than 10 m.

Here, the presence of a low resistivity anomaly, shown in the gravel layer, may stem from water leakage from the pond. A comparison of VES and RIP results indicates that the interpreted resistivity of the gravel layer shown in the VES result is greater than that estimated from the RIP. A leakage or infiltration of water directly from the bottom of the pool to the underlying laterite and gravel layers may have resulted in the layers beneath the water's bottom being wetter than their surrounding areas. Therefore, the resistivity of the gravel layer underneath the pond bottom is less than that of layers near the pond.

3.2 Lake Test Site

The Chung-Dah Lake, located in the campus of National Central University, was selected as the second test site. Geological conditions were about the same as for the pond site except the thickness of laterite here is about 3 to 4 m and the thickness of the gravel ranges from 12 to 15 m. The bottom of the lake was covered with thin sludge. An E-W survey line of 31 m in length was set at the SW corner of the lake. Fifteen meters of this survey line was placed in the lake while the rest of the line remained on land. The GPR survey was only conducted on the water surface along the survey line. In contrast, the RIP survey was conducted on both the water's surface and the land along the survey line.

Figure 3a shows the GPR image of this survey line. An obvious reflection from the lake bottom can be recognized. The water depth was about 1 m and became shallower toward the western end of the section because this western side is close to the bank. The apparent resistivity pseudosection (Fig. 3b) indicates resistivity increasing as the depth increases, except at a distance of 5 to 14 m which was affected by pebbles on the bank. Water resistivity was around 80 ohm-m given by performing resistivity measurement with a small Wenner array on the water surface. Consequently, the low resistivity zone shown in Fig. 3c, extending from the water surface to a depth with resistivity of 80 ohm-m, is interpreted as the water body. The layer underneath the lake bottom is laterite with a thickness less than 2 m and resistivity ranging from 80 to 200 ohm-m. The stratum beneath the laterite is water-saturated gravel with a

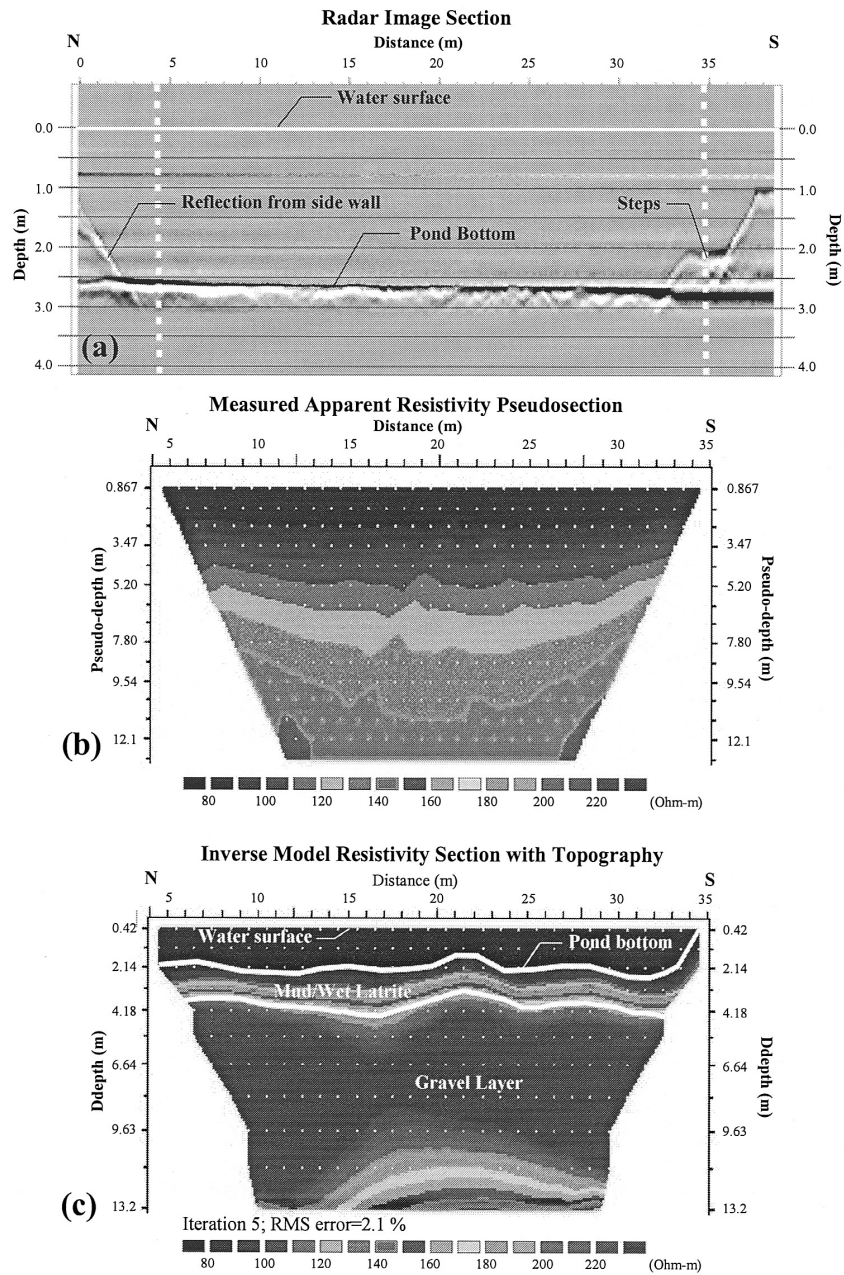


Fig. 2. GPR and RIP results collected at the pond site. (a) Radar image section, (b) apparent resistivity pseudosection, and (c) inverted resistivity depth section.

thickness ranging from 9 to 13 m and a resistivity higher than 200 ohm-m. The high resistivity zone between 5 to 14 m shown in Fig. 3c reflects the effect of the bank consisting of aggregated pebbles. As shown in Fig. 3c, the influence of the bank effect on the western side decreased. A low resistivity laterite region on top of gravel layers is indicated here except for a high resistivity zone associated with the pavement between 0 to 5 m.

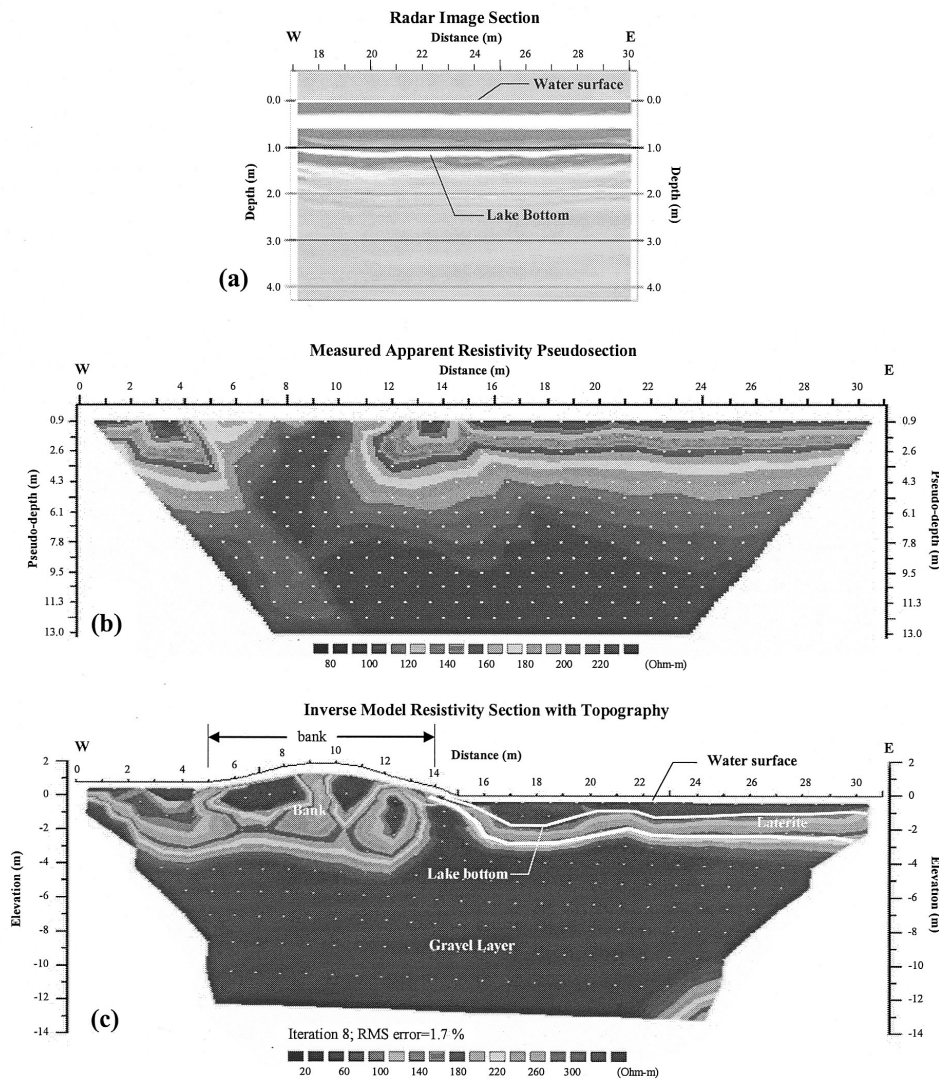


Fig. 3. GPR and RIP results collected at lake site. (a) Radar image section, (b) apparent resistivity pseudosection, (c) inverted resistivity depth section.

4. MAPPING AN ACTIVE FAULT ALONG A RIVER CHANNEL

The Hsincheng fault is located in Hsinchu County, northwestern Taiwan. It is a thrust fault moving in a NE-SW direction with a length of about 18 km and a SE 40 degree dip. The inferred Hsincheng fault trace lies in a region between axes of the Chintsohu anticline and Paoshan anticline. Formations in the SE part of the fault consist mainly of alternating Pliocene Cholan shale and sandstone, while those of the NW part are mainly massive sandstone and sandstone/mudstone alternations with intercalated thin conglomerate layers of Pleistocene Toukoshan Formation. The southeastern block thrust over the northwestern block during faulting. Some studies show that the Hsincheng fault displaced not only Pleistocene lateritic terrace deposits but also recent non-lateritic deposits, and suggest that the Hsincheng fault was once reactivated along the old fault plane (Hsu 1986). Huang (1984) reports ten fault outcrops. Besides this description, the outlook and property of rocks on both sides are largely similar.

In 1997, a typhoon caused a flood in the Tourochyan River, during which vast quantities of river sediments were washed out to sea, and parts of the previously buried outcrops of Hsincheng, at the river's bottom, were exposed above the water surface. The location of the exposed fault is in northeast Ellchorngpun, 500 m from Chuibeei city. The stratigraphic units exposed in the study area include the Yangmei Formation, Toukoshan Formation, terrace deposits and alluvium. The Quaternary laterite deposit and non-lateritic terrace were offset by the Hsincheng thrust fault, a linear fault-line scarp crossing the Tourochyan River. The thrust fault strikes N55°E and dips at a 60 degrees angle to the southeast. The hanging wall is characterized by the Chaochin Member of Yangmei Formation, consisting of siltstone and mudstone. The footwall is the Chaomen Member of Yangmei Formation and has inter-bedded sandstone and mudstones (Shih et al. 2003). An underwater fault can be traced from the outcrops rising above the surface of the nearby river. This provided a good opportunity to test the reliability of mapping the underwater fault using geoelectrical methods.

The resistivity measured from both sides of the fault's outcrop indicates that the footwall has an average resistivity of 18.5 ohm-m, and the hanging wall has an average resistivity of 11.3 ohm-m. The resistivity measured at the fault fracture zone was around 11 ohm-m. The resistivity of the footwall was generally higher than that of the hanging wall. The presence of lower resistivity at the hanging wall and fault trace was caused partially by the low resistivity of the constituent rocks and partially by water saturated fractures resulting from compression of faulting in the hanging wall.

To evaluate the ability of the new survey strategy to map faults, three survey lines were set up in this site, as shown in Fig. 4. L1 was perpendicular to the strike of the Hsincheng fault. L2 and L3 were parallel to the fault strike at a distance of 20 m and 10 m from the fault trace, respectively. L2 was in Hsincheng fault's footwall and L3 was in its hanging wall. All the GPR measurements for these profiles were carried out on the water's surface. However, for the RIP, only some of the electrodes were deployed on the water surface; the survey line L2 had an electrode on the water's surface extending from -2 to 17 m, while L3 extended from 0 to 12 m.

Figures 5a, b and c show the results of line L1. As shown in Fig. 5a, the bottom of the river was clearly described from the radar image section. However, in this study site, no obvious

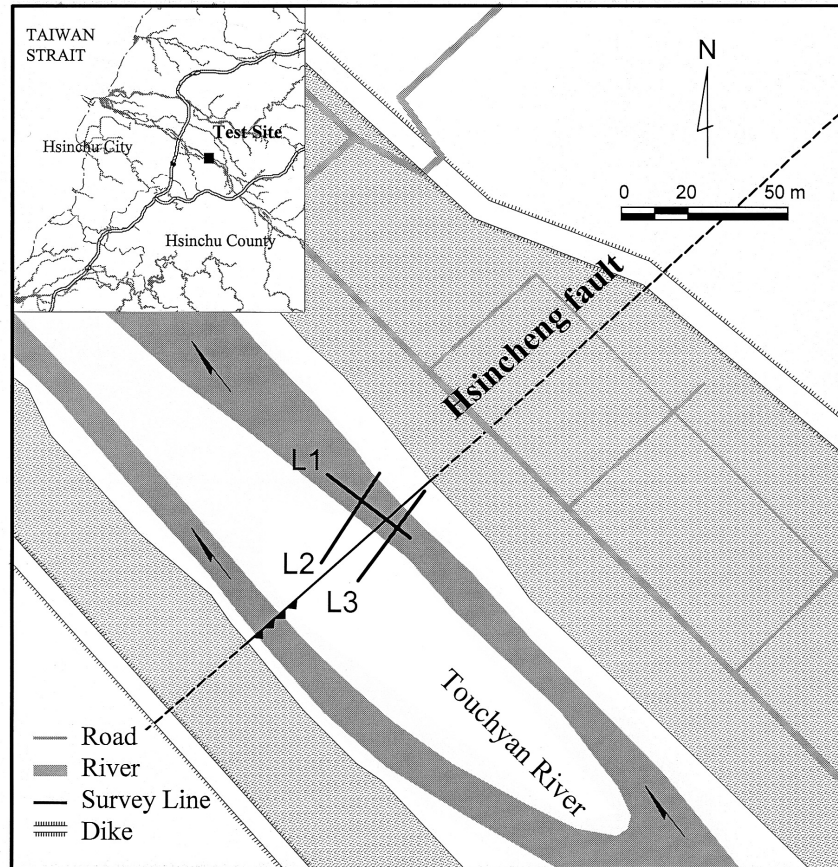


Fig. 4. Location of survey lines at Touchyan River channel.

reflection beneath the river bottom could be recognized. The main fracture zone of Hsincheng fault was labeled in Fig. 5a by referring to the surface fault trace and outcrops. As shown in Fig. 5a, the continuous and strong reflection on the northwestern side possibly indicates the presence of inter-layered conglomerate, sandstone and mudstone. The weak reflection, around the horizontal position labeled 25 to 34 m with a depth of 2 to 2.25 m, may be caused by decreasing the dielectric contrast between the water and riverbed. The increase in the dielectric constant of the riverbed in this region may be due to an increase in water saturation in the formation and perhaps related to fracture formation.

The apparent resistivity pseudosection (Fig. 5b) shows resistivity in the NW side (footwall) being higher than on the SE side (hanging wall). This is consistent with the resistivity measured from outcrops as mentioned above. Figure 5c is the inverted resistivity depth profile from Fig. 5b. An obvious feature of a high-angle discontinuous resistivity zone with an appar-

ent dip about 68° SE can be recognized near 30 to 34 m in Fig. 5c. This discontinuous resistivity zone was located right in the extension of the known fault trace and extends downward to a depth greater than 13 m. It may be related to the fracture zone of the Hsincheng fault. This result is comparable with the GPR result.

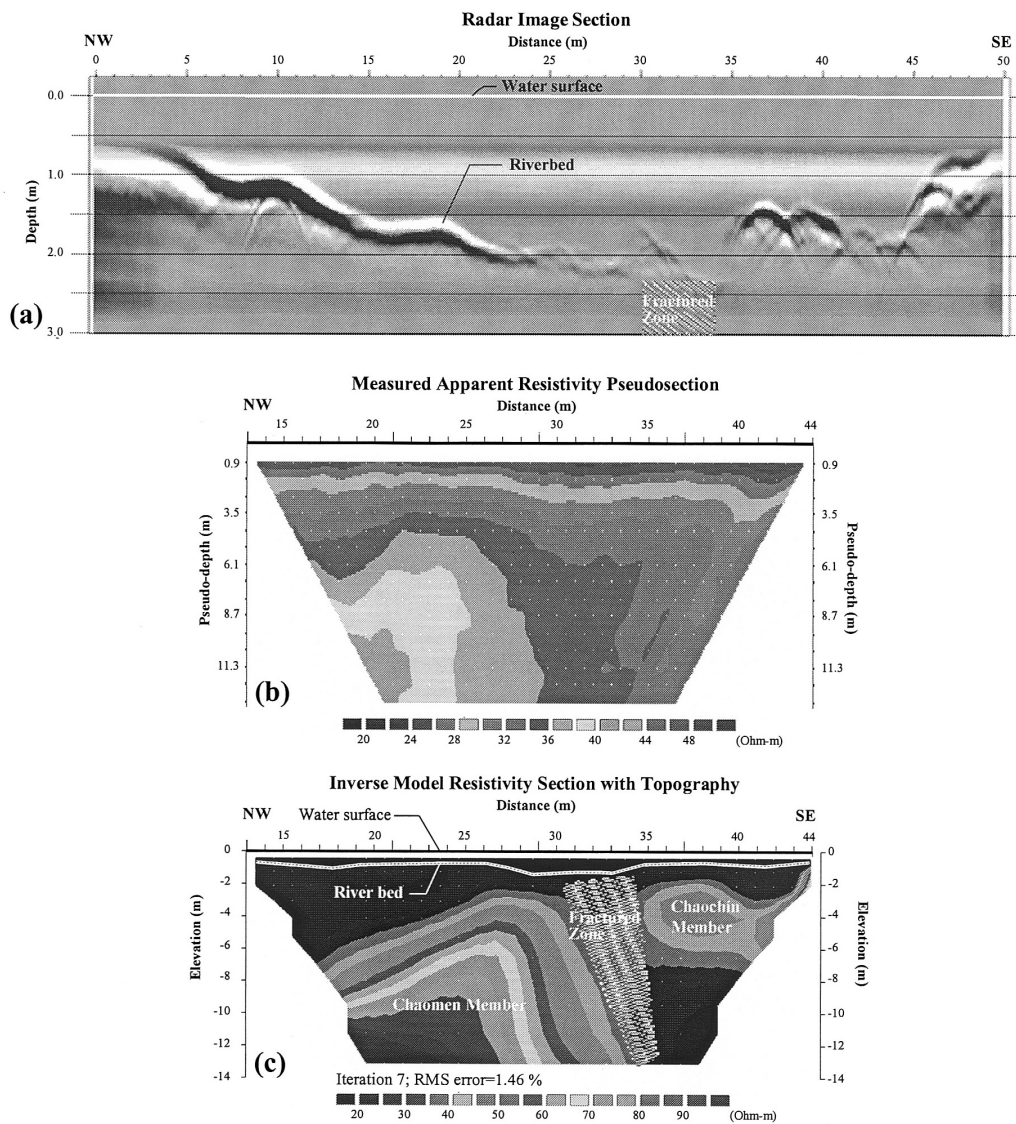


Fig. 5. GPR and RIP results for survey line L1. (a) Radar image section, (b) apparent resistivity pseudosection, (c) inverted resistivity depth section.

The features of the electric responses shown in both the GPR and RIP sections for line L2 and L3 are not similar to the profile images shown in Fig. 5. Figures 6a, b and c are the GPR and RIP sections of L2. The higher resistivity zone in the SW side of Fig. 6c is associated with the riverbank. Figures 7a, b and c are the GPR and RIP sections of L3. Except for the higher resistivity zones beneath the river bottom, which may have been caused by fluvial sediments, the average resistivity of line L2 (hanging wall) is lower than the average resistivity of L3

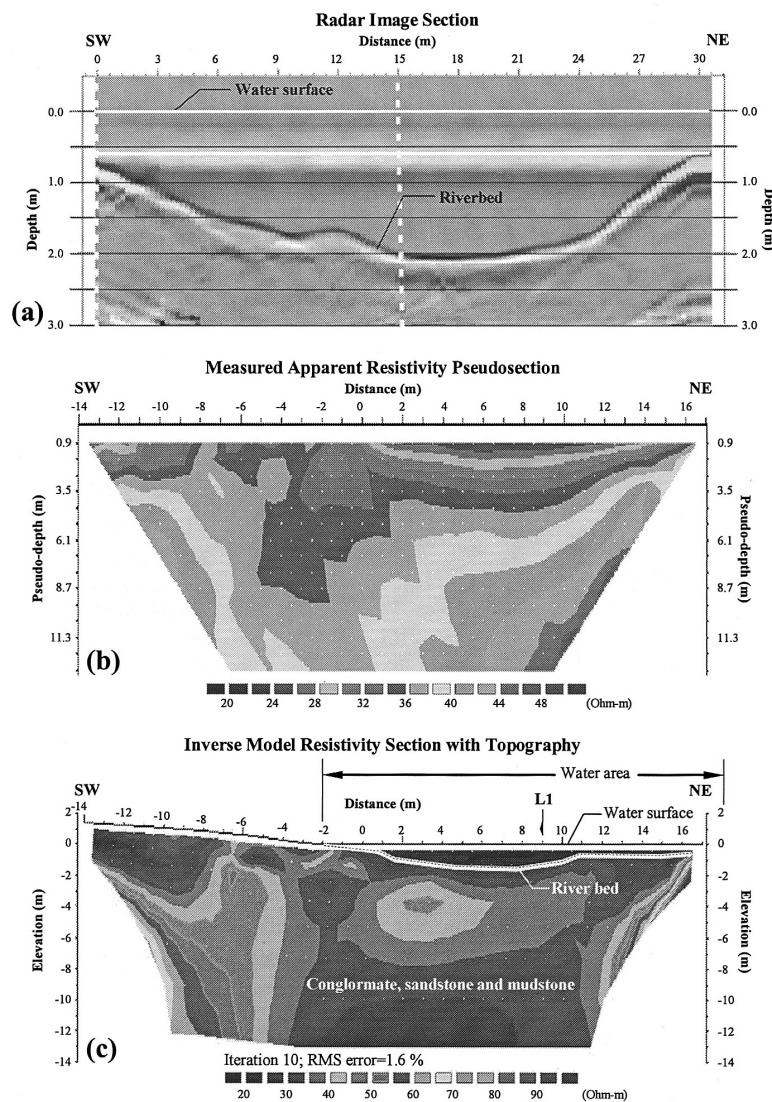


Fig. 6. GPR and RIP results for survey line L2. (a) Radar image section, (b) apparent resistivity pseudosection, (c) inverted resistivity depth section.

(footwall). Resistivity decreased as depth increased, with the exception of a local high resistivity zone on the NE riverbank. Lateral resistivity variation of the fluvial sediments beneath the water bottom may relate to saturation changes in the sediment. However, no obvious electric discontinuous zones are found in these figures.

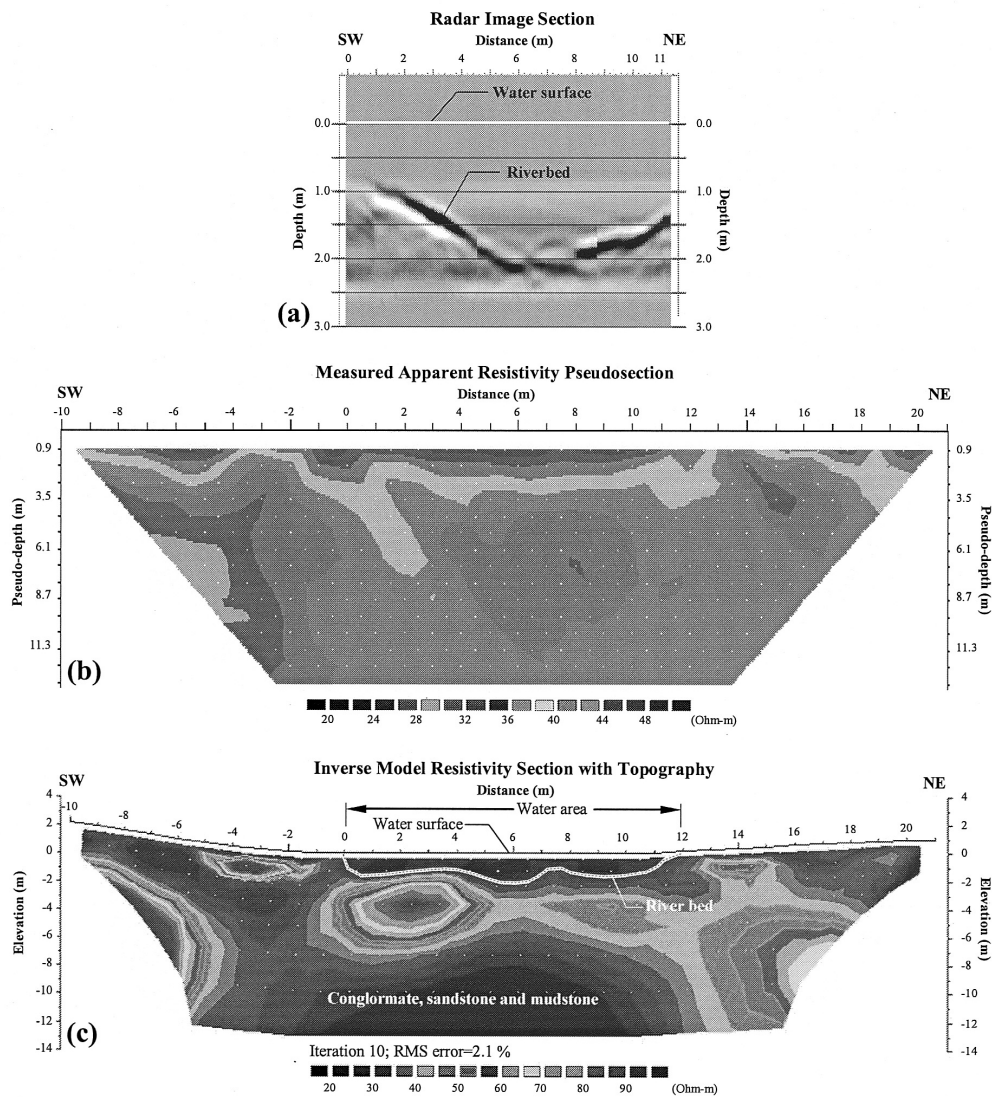


Fig. 7. GPR and RIP results for survey line L3. (a) Radar image section, (b) apparent resistivity pseudosection, (c) inverted resistivity depth section.

5. CONCLUSIONS

Although geoelectric signals are often distorted in an underwater environment, this preliminary study shows that GPR and RIP surveys can be integrated to successfully provide details on geological structures beneath water layers. The estimated water depth gleaned from RIP is usually less accurate than that taken from GPR. The penetrating power of GPR is not high, but it provides both bathymetry and shallow stratigraphy to compensate for resistivity processing and interpretation. Arguably, integrated use of GPR and RIP provides a better picture of underwater stratigraphy.

The results of this study demonstrate that integrated use of GPR and RIP at the water surface is an improved means of detecting geological structures beneath the water bottom. An additional benefit is that this survey strategy can be employed to map subsurface structures in areas where seismic methods are difficult; for example, river surfaces, reservoir and drainage canals. This innovative method suggests an exciting new approach to conducting geophysical surveys along rivers and drainage canals and in urban areas, places where roads and buildings impede other methods designed to detect active faults.

Acknowledgements This study was supported by the National Science Council grant (NSC87-2116-M008-014), Republic of China. The authors thank the geoelectric group of National Central University for their help with the field-work.

REFERENCES

- Annan, A. P., and J. L. Davis, 1977: Impulse radar applied to the thickness measurements and freshwater bathymetry. *Geol. Surv. Canada, Paper 77-1B*, 63-65.
- Belaval, M., J. W. Lane, Jr., D. P. Lesmes, and G. C. Kineke, 2003: Continuous-resistivity profiling for coastal groundwater investigations: three case studies, *Symp. Appl. Geophys. Eng. Environ. Prob. (SAGEEP)*, 14 pp.
- Delaney, A. J., P. V. Sellmann, and S. A. Arcone, 1992: Sub-bottom profiling: a comparison of short-pulse radar and acoustic data. *Spec. paper 4th Int. Conf. on GPR*, 149-157.
- Griffiths, D. H., and R. D. Barker, 1993: Two-dimensional resistivity imaging and modelling in areas of complex geology. *Appl. Geophys.*, **29**, 211-226.
- Huang, C. S., 1984: Quaternary faults in the coastal area between Hsinchu and Chunan, north-western Taiwan. *Spec. Publ. Cent. Geol. Surv.*, **3**, 103-126.
- Hsu, T. L., 1986: *Geology and Engineering*. Ker-Chi Book Company, Taipei (in Chinese).
- Kwon H, S., J. H. Kim, H. Y. Ahn, J. S. Yoon, K. S. Kim, C. K. Jung, S. B. Lee, and T. Uchida, 2005: Delineation of a fault zone beneath a riverbed by an electrical resistivity survey using a floating streamer cable. *Expl. Geophys.*, **36**, 50-58.
- Loke, M. H., and R. D. Barker, 1996: Rapid least-squares inversion of apparent resistivity pseudosections by a quasi-Newton method. *Geophys. Prosp.*, **44**, 131-152.
- Loke, M. H., 2000: Electrical imaging surveys for environmental and engineering studies, web site, (www.geoelectrical.com).

- Lmai, T., T. Sakayama, and T. Kanemori, 1987: Use of ground-penetrating radar and resistivity surveys for archeological investigations. *Geophys.*, **52**, 137-150.
- Savvaidis, A., G. Tsokas, Y. Liritzis, and M. Apostolou, 1999: Location and Mapping of Ancient Ruins on the Castle of Lefkas (Greece) by Resistivity and GPR Methods. *Archaeol. Prosp.*, **6**, 63-73.
- Shih, T. S., S. T. Lu, W. H. Lin, and Y. H. Lee, 2003: A Study on the Location and Activity of the Hsincheng Fault. *Spec. Publ. Cent. Geol. Surv.*, **14**, 37-52.

Yang, C. H., Tong, L. T., and Yu, C. Y., 2006: Integrating GPR and RIP methods for water surface detection of geological structures. *Terr. Atmos. Ocean. Sci.*, **17**, 391-404.